Device physics of organic bulk heterojunction solar cells

Mihailetchi, V.D

2

Charge transport in polymer:fullerene films*

Abstract

For the understanding of the opto-electronic properties of MDMO-PPV:PCBM solar cells, knowledge about the charge transport properties is indispensable. In this chapter, the electron transport through spin cast PCBM films is investigated as a function of temperature. The occurrence of a space-charge limited current enables a direct determination of the electron mobility from current-voltage characteristics. The resulting electron mobility in the acceptor-type PCBM is found to be more that three orders of magnitude larger than the hole mobility measured in the pristine donor-type MDMO-PPV. The observed temperature dependence of the electron mobility in pristine PCBM films can be described using correlated Gaussian disorder model, which provides information about the energetic disorder in PCBM. Moreover, it is demonstrated that in order to electrostatically allow the experimentally observed photocurrents in MDMO-PPV:PCBM blends, a hole mobility in the MDMO-PPV phase of the blend of more than two orders of magnitude higher is required, as compared to the hole mobility of pristine MDMO-PPV. The space-charge limited conduction, admittance spectroscopy, and transient electroluminescence measurements reveal that hole mobility in the MDMO-PPV phase of the blend is enhanced by a factor of 400 in the presence of PCBM. Consequently, the charge-carrier transport in the MDMO-PPV:PCBM solar cells is much more balanced than previously assumed, which is a necessary requirement for the reported high fill factors of typically above 50%, and the high photon-to-electron conversion efficiencies.

*The main results of this chapter have been published as: (a) V. D. Mihailetchi, J. K. J. van Duren, P. W. M. Blom, J. C. Hummelen, R. A. J. Janssen, J. M. Kroon, M. T. Rispens, W. J. H. Verhees, M. M. Wienk, *Advanced Functional Materials* **13** (2003), 43; (b) C. Melzer, E. J. Koop, V. D. Mihailetchi, P. W. M. Blom, *Advanced Functional Materials* **14** (2004), 865.

2.1 Photoconduction in insulators

In first-order approximation, a polymer:fullerene bulk heterojunction solar cell can be regarded as an insulator sandwiched between two electrodes. The light entering the transparent electrode is considered to be uniformly absorbed by the active layer, which results in a uniform generation of electron-hole pairs throughout the specimen. In reverse bias the contacts inject negligible current compared with the volume photogenerated current by absorption of light. The lateral dimensions of the active layer are large compared to its thickness (L), so that the problem is one dimensional. In addition, diffusion current superimposed on drift current is at first neglected and the charge carrier mobility is assumed to be independent of the electric field at low electric fields, where these solar cells operate. Following charge separation at the internal donor/acceptor interface, free electrons are transported by hopping via percolated fullerene molecules towards the negative electrode and holes via the polymer network to the positive electrode. Therefore, only the LUMO level of fullerene and the HOMO level of the polymer are considered as effective conduction and valence band in the metal-insulator-metal (MIM) treatment, as is used to investigate these devices.

Under the above considerations, the recombination probability of the free charge carriers in photovoltaic cells depends on the mean carrier drift length $w_{e,h}$=$\mu_{e,h}\tau_{e,h}E$ of electrons (e) and holes (h), respectively [1, 2]. Here, μ is the charge carrier mobility, τ is the charge carrier lifetime before trapping or recombination, and E is the electric field. If the mean carrier drift lengths of electrons and holes are smaller than the device thickness L ($w_{e,h} < L$), then both charge carriers are accumulated in the layer. At steady state, the distance which they travel increases linearly with applied voltage (V) and the photocurrent J_{ph} follows Ohm's law [2]:

$$J_{ph} = qG(\mu_e\tau_e + \mu_h\tau_h)\frac{V}{L}, \tag{2.1}$$

where q is the electric charge and G is the generation rate of electron-hole pairs.

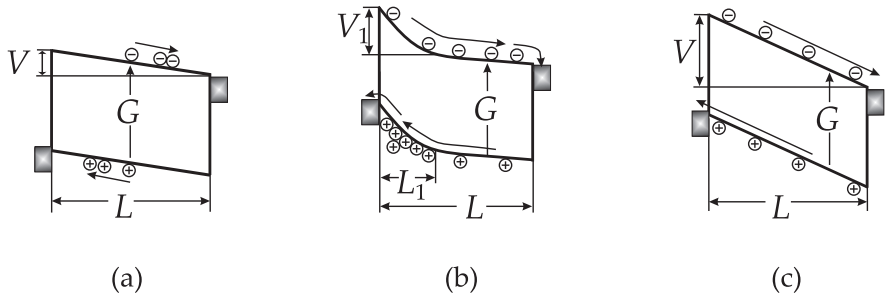

Figure 2.1: Schematic energy-band diagrams of a photovoltaic device upon illumination with applied voltage V between the contacts. Energy-band diagram when both $w_{e,h} < L$ (a), under hole accumulation regime when $w_h < L$ and $w_e \geq L$ (b), and in the saturation regime when both $w_{e,h} \geq L$ (c).

This situation is schematically shown in Figure 2.1(a). It is obvious that the photoconductivity gain is maximized when the field reaches a value at which both mean carrier drift length exceeds the device thickness, or in other words, the lifetime τ of photogenerated charges exceeds their transit time. In this case, all photogenerated free charge carriers are extracted at the contacts and the photocurrent is saturated (J_{ph}=qGL) [1, 2], as shown in Figure 2.1(c).

As pointed out by Goodman and Rose [1], an interesting solution exists in the case of very different mobility lifetime products of the charge carriers (e.g., $\mu_e\tau_e \gg \mu_h\tau_h$). In a semiconductor with $w_e \gg w_h$ and $w_h < L$, the holes will accumulate to a greater extent in the device than the electrons, which makes the applied field non-uniform. As a consequence, the electric field increases in the region (L_1) near the anode, enhancing the extraction of holes, as shown schematically in Figure 2.1(b). Conversely, in the region near the cathode the electric field decreases, diminishing the extraction of electrons. In the steady-state, the electric field in the region with thickness L_1 is modified to such an extent that the external hole current equals the external electron current. Based on the dominant electronic processes that occur in the layer, Goodman and Rose predicted the photocurrent density J_{ph} as a function of the applied voltage V, for the above consideration, to be [1]:

$$J_{ph} = qGL(1+b)\frac{-b + \left(b^2 + 4(1-b)V\mu_h\tau_h/L^2\right)^{1/2}}{2(1-b)}, \tag{2.2}$$

where b is the drift length ratio (defined here as $\mu_h\tau_h/\mu_e\tau_e$). For equal electron and hole $\mu\tau$ products ($b = 1$), it can be seen that Equation 2.2 reduces to Equation 2.1 and at higher voltages the photocurrent saturates at qGL [1]. According to Equation 2.2, for very different charge transport properties of electrons and holes ($1 \gg b \to 0$), the J_{ph} approaches one-half power on V:

$$J_{ph} = qG(\mu_h\tau_h)^{1/2}V^{1/2}. \tag{2.3}$$

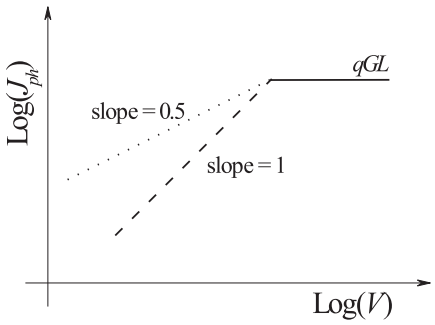

Figure 2.2: Schematic representation of the photocurrent-voltage (J_{ph}-V) dependence when both $w_{e,h} < L$ (dashed line), the hole accumulation regime when $w_h < L$ and $w_e \geq L$ (dotted line), and in the saturation regime when both $w_{e,h} \geq L$ (solid line).

Hence, it is interesting to examine some special or limiting cases of the solution of Equation 2.2: for equal electron and hole drift lengths ($\mu_e\tau_e$=$\mu_h\tau_h$, i.e., b=1), only the linear and saturation regime of $J_{ph}(V)$ are possible. For very different charge transport properties of electrons and holes (e.g. $\mu_e\tau_e \gg \mu_h\tau_h$, i.e., $1 \gg b \rightarrow 0$), the $J_{ph}(V)$ dependence is dominated by the square-root and saturation regimes. Figure 2.2 shows the $J_{ph}(V)$ dependence of these two limiting cases.

In the polymer:fullerene blends, charge transfer at the donor/acceptor interface produces free electrons and free holes in the two materials. Subsequently, the electrons and holes are extracted at the corresponding electrodes or recombine bimolecularly. This last process results in an equal electron and hole lifetime, since when an electron disappears also a hole disappears from the device. Hence, in that case an eventual difference in their $\mu\tau$ products mainly originates from a difference in charge carrier mobility. Therefore, determining the charge carrier mobilities is a crucial step in understanding the photocurrent-voltage characteristics of these solar cells.

2.2 Electron transport in fullerene films

2.2.1 Introduction

A promising combination of material for a plastic solar cell is the donor-type conjugated polymer MDMO-PPV and acceptor-type molecules such as the C_{60} derivative PCBM [3]. As a concept a bulk heterojunction is used, which consists of a three dimensional interpenetrating donor-acceptor network, sandwiched between two electrodes with different work functions to generate an electric field across the organic layer. For these kind of cells a power conversion efficiency of 2.5% under AM 1.5 illumination has been reported [4, 5]. From photophysical studies it has been demonstrated that after absorption of a photon, ultra-fast electron transfer takes place from the excited state of a conducting polymer to acceptor molecules such as Buckminster fullerenes (C_{60}), with a quantum efficiency close to unity [6, 7]. Subsequently, the separated charge carriers are transported via the interpenetrating network to the electrodes. The photogenerated current is directly governed by the charge carrier mobility, as is demonstrated in the previous section, alongside the number of photoexcited charge carriers.

For the understanding of the opto-electronic properties of MDMO-PPV:PCBM solar cells, knowledge about the charge transport properties of the individual components is indispensable. For MDMO-PPV the transport of holes has been extensively studied due to its application in polymer light-emitting diodes. From dark current density-voltage (J_D-V) measurements [8], transient electroluminescent measurements [9], and impedance spectroscopy [10], a hole mobility $\mu_h = 5 \times 10^{-11}$ m^2/Vs has been obtained for MDMO-PPV at room temperature. The field- (E) and temperature (T) dependence of the hole mobility in PPV was described by a stretched exponential dependence

$$\mu(E,T) = \mu_0(T)\exp(\gamma(T)\sqrt{E}), \tag{2.4}$$

where $\mu_0(T)$ is the zero-field mobility and $\gamma(T)$ describes the field activation [8–10]. However, recent developments have shown that, the application of Equation 2.4 to describe the electric field dependence of the charge carrier mobility in low mobility media is not fully correct due to the fact that the density dependence of charge carrier mobility has been neglected [11–13]. Therefore, the values of γ at high electric fields are overestimated. In this section, the zero-field mobility of electrons in pristine PCBM films is investigated.

2.2.2 Results and Discussion

The devices under investigation consist of a single PCBM layer sandwiched between a hole-conducting layer of PEDOT:PSS, typically of 100 nm thickness, and an evaporated lithium fluoride (LiF; ≈1 nm)/ aluminum (Al; ≈100 nm) top electrode (see Section 2.4). In the inset of Figure 2.3, an energy band diagram of the device is shown under flat-band condition.

From the work functions, it is expected that LiF/Al forms an Ohmic contact for electron injection into PCBM. The work function of PEDOT:PSS (5.2 eV) does not match the HOMO level of PCBM (6.1 eV) [3], thus hole injection from PEDOT:PSS into PCBM can be neglected. Consequently, only electrons are expected to flow through PCBM under forward bias conditions. Furthermore, from the energy band diagram at room temperature a built-in voltage V_{BI} of around 1.5 V is expected. The J_D-V measurements are performed in nitrogen atmosphere within a temperature range of 150-300 K. With deceasing temperature V_{BI} is expected to typically increase by 0.3 V in the range 300-150 K, due to diffusion of thermally injected charges [14]. The active area amounts to 10^{-5} m^2. In Figure 2.3, the experimental J_D-V characteristics at room temperature (295 K) are shown for PCBM devices with layer thicknesses, L, of 90 nm and 170

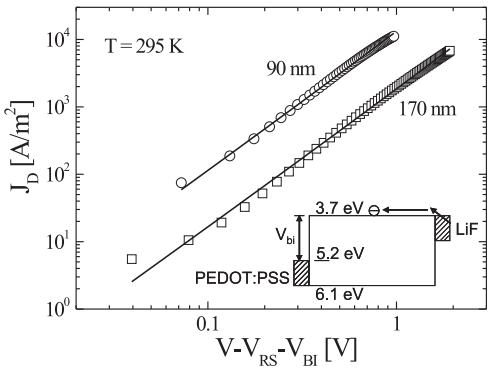

Figure 2.3: Experimental (symbols) and calculated (solid lines) J_D-V characteristics of ITO/PEDOT:PSS/PCBM/LiF/Al devices with thicknesses L=90 nm and 170 nm, using V_{BI}=1.4 V and RS=30 Ω. The device band diagram is indicated in the inset. The electron transport is described by SCLC (Equation 2.5) with an electron mobility $\mu_e = 2.0 \times 10^{-7}$ m^2/Vs and a dielectric constant ϵ_r=3.9.

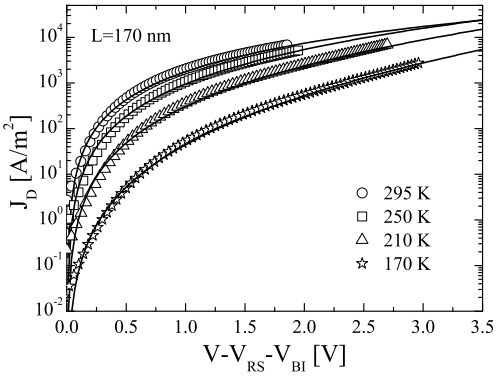

Figure 2.4: Experimental J_D-V characteristics of an ITO/PEDOT:PSS/PCBM/LiF/Al device with thickness L=170 nm for various temperatures (symbols). The solid lines represent the calculated J_D-V characteristics as predicted by a SCLC model using the field-dependent mobility defined by Equation 2.4.

nm.

Using V_{BI}=1.4 V it is observed from the slope of the log(J_D) versus log(V) plot that the current density J_D depends quadratically on voltage. This behavior is characteristic for a space-charge limited current (SCLC) given by [15]

$$J_D = \frac{9}{8}\epsilon_0\epsilon_r\mu_e\frac{V^2}{L^3}, \tag{2.5}$$

where $\epsilon_0\epsilon_r$ is the permittivity of PCBM. From capacitance-voltage measurements we have obtained a relative dielectric constant ϵ_r of 3.9 for PCBM. Using ϵ_r=3.9, we find that the J_D-V characteristics of our devices with L=90 and 170 nm are well described by Equation 2.5, with $\mu_e = 2.0 \times 10^{-7}$ m^2/Vs. Thus, the observation of SCLC provides direct information on the electron mobility in PCBM. It should be noted that for current densities larger than 1000 A/m^2, the applied voltage should be corrected for the voltage drop across the ITO series resistance (V_{RS}), which typically amounts to 25-30 Ω in our substrates. An important conclusion is that, at room temperature, the electron mobility of PCBM is a factor of 4000 larger than the hole mobility of pristine MDMO-PPV [8–10]. The observed electron mobility of 2.0×10^{-7} m^2/Vs in PCBM is a factor of 40 less than mobilities reported from field-effect measurements on thin films of evaporated C_{60}, which are typically 8×10^{-6} m^2/Vs [16]. For C_{60} single-crystals grown from the vapor phase, mobilities of 5×10^{-5} m^2/Vs have been measured by time-of-flight experiments [17]. The reduction of the mobility in PCBM films as compared to C_{60} single crystals indicates that disorder may play an important role in PCBM thin films.

Figure 2.4 shows the J_D-V characteristics of a PCBM device with L=170 nm as a function of temperature. In order to describe the electron current in PCBM, the SCLC model is combined with the field-dependent mobility of Equation 2.4.

The J_D-V characteristics of the PCBM device are now characterized by the following equations [15]

$$J_D = qn(x)\mu_e[E(x)]E(x) \tag{2.6}$$

$$\frac{\epsilon_0\epsilon_r}{q}\frac{dE(x)}{dx} = n(x), \tag{2.7}$$

where q is the electric charge, and $n(x)$ is the density of electrons at position x. Assuming Ohmic contacts (x=0), we have the boundary condition $n(0)$=N_c, with the effective density of states in the conduction band, N_c=2.5 $\times$ 10^{25} m^{-3} [8]. Equations 2.4, 2.6 and 2.7 can be solved numerically for a given electron current density J_D. The voltage is given by

$$V = \int_0^L E(x)dx \tag{2.8}$$

The built-in voltage V_{BI} has been gradually increased from 1.4 V (295 K) to 1.7 V (150 K) [14]. From Figure 2.4 it appears that the dependencies of E and T on the J_D-V characteristics are consistently described by the combination of SCLC and the empirical mobility given by Equation 2.4.

This empirical mobility appears to be generic for a large class of disordered materials [18] such as molecularly doped polymers, pendant-group polymers, conjugated polymers, and organic glasses. This suggests that the conduction mechanisms in these various material systems are identical. It has been demonstrated from Monte-Carlo simulations that hopping between sites that are subject to positional and energetic disorder reproduces the stretched exponential field dependence of the empirical mobility (Equation 2.4) [19]. In these calculations, the site energy distribution is assumed to be Gaussian, and characterized by a width, σ. This Gaussian density of states (DOS) reflects the energetic spread in the transport sites due to disorder. Taking into account long-range spatial energy correlation improves the agreement between the simulations and the empirical $\mu \propto \exp(\gamma\sqrt{E})$ behavior at low electric fields [20]. At high electric fields, however, the dependence on charge carriers density must be taken into account [11–13]. Such energy-correlation may originate from charge-dipole interactions in the material. From these simulations a mobility of the following form has been proposed

$$\mu = \mu_\infty \exp\left[-\left(\frac{3\sigma}{5k_BT}\right)^2 + 0.78\left(\left(\frac{\sigma}{k_BT}\right)^{3/2} - \Gamma\right)\sqrt{\frac{qaE}{\sigma}}\right], \tag{2.9}$$

where μ_∞ is the mobility at the limit $T \to \infty$, σ is the width of the Gaussian DOS, a is the intersite spacing, k_B is Boltzmann's constant, and Γ is the positional disorder of the transport sites. The coefficient Γ equals 2 for a regular lattice [20], but is greater for a system with randomly located molecules.

From the J_D-V characteristics as shown in Figure 2.4 the temperature dependence of μ_0 is determined. According to Equation 2.9, the slope of a plot of the zero field-mobility $\mu_0 \propto T^{-2}$ would then directly provides a value for σ. In Figure 2.5, the experimental μ_0 is plotted against T^{-2}. For σ=73 meV, the prediction of the disorder model are in excellent agreement with the experimental

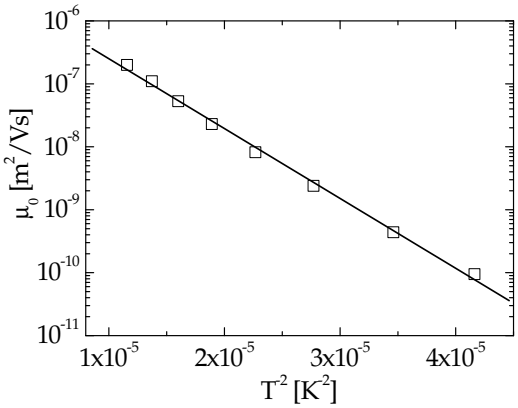

Figure 2.5: Temperature dependence of the zero-field mobility μ_0 of PCBM as obtained from the J_D-V characteristics shown in Figure 2.4. The solid line represents the calculated μ_0 according to the disorder model (Equation 2.9), as explained in the text.

electron mobilities. From the same analysis as applied to the hole mobility of MDMO-PPV, σ=110 meV have been reported [21]. The lower thermal activation and resulting smaller σ of PCBM as compared to MDMO-PPV, demonstrates that the energetic disorder is significantly smaller in PCBM, which gives rise to a higher mobility. In conjugated polymers as MDMO-PPV the energetic disorder will be enhanced by fluctuations in the length of the transporting conjugated chain segments.

2.2.3 Conclusion

The electron transport in PCBM has been studied by means of J_D-V measurements. At room temperature, the PCBM electron mobility exceeds the hole mobility of pristine MDMO-PPV by more than three orders of magnitude. The temperature dependence of the electron mobility of PCBM is described using the correlated Gaussian disorder model. This model provides information on the microscopic transport parameters. The enhanced electron mobility of PCBM as compared to the hole mobility in pristine MDMO-PPV films is due to less energetic disorder in PCBM.

2.3 Electron and hole transport in polymer:fullerene blends

2.3.1 Introduction

In blends of MDMO-PPV and PCBM, after photoinduced electron transfer at the donor/ acceptor interface [6, 7], the photogenerated free holes and electrons are subsequently transported through the donor (MDMO-PPV) and acceptor

(PCBM) phases to the anode and cathode, respectively, resulting in an external photocurrent density J_{ph}. Since the photocurrent is not solely governed by the generation rate G of free electron-hole pairs, but also by recombination processes, the charge-transport properties of the semiconductor are determinative for an efficient photoresponse. As shown in Section 2.1, the recombination of the free charge carriers is significant, if the mean carrier drift length w of one or both charge-carrier species is smaller than the device thickness L. In other words, recombination is important as long as the transit time of the photogenerated charge carriers is longer than their lifetime. However, if both mean carrier drift lengths exceed the thickness of the film (L), no recombination occurs and the electrodes extract all photogenerated charge carriers. In this saturation regime, both electron and hole lifetimes equal the transit times of the charge carriers and the photocurrent density is saturated ($J_{ph}^{sat} = qGL$) [1, 2, 22].

Since the hole mobility of pristine MDMO-PPV has previously been reported to be 5×10^{-11} m^2/Vs [8–10], whereas an electron mobility for PCBM of 2×10^{-7} m^2/Vs has been determined in Section 2.2, the charge transport in heterojunction photovoltaic cell based on these materials is expected to be strongly unbalanced ($\mu_e \gg \mu_h$). This has deep impact on the photoresponse of the respective cell, as demonstrated in Section 2.1. Due to the unbalanced charge-transport properties, holes accumulate to greater extent in the device than electrons do, as shown in Figure 2.1(b). Under steady-state conditions, the electric field in region with thickness L_1 is modified to such an extent that the external hole current equals the external electron current. However, in the region L_1, electrons do not neutralize the accumulated holes, which results in build-up of positive space-charge. The electrostatic limit of hole accumulation is reached when the photogenerated current density $J_{ph1} = qGL_1$ is equal to the space-charge-limited current density in region L_1 [1]:

$$J_{ph1} = qGL_1 \leq J_{SCLC1} = \frac{9}{8}\epsilon_0\epsilon_r\mu_h\frac{V_1^2}{L_1^3}, \tag{2.10}$$

where J_{SCLC1} is the space-charge-limited current density across the region of strong hole accumulation, V_1 is the voltage drop over this region, and $\epsilon_0\epsilon_r$ is the dielectric permittivity. Since almost the entire voltage V drops in the region of hole accumulation ($V_1 \approx V$), the maximal electrostatically allowed photocurrent density J_{ph}^{max} is given by [1]:

$$J_{ph} \leq J_{ph}^{max} = (qG)^{0.75}\left(\frac{9}{8}\epsilon_0\epsilon_r\mu_h\right)^{0.25}\sqrt{V} \tag{2.11}$$

Note that J_{ph}^{max} scales with the square-root of the voltage and depends on the charge carrier mobility of the slowest charge carrier species as well as the generation rate of free electron-hole pairs. A more detailed analysis of this is given in Section 3.2 of this thesis. In order to be able to predict the electrostatic limit, information on G is still required. The magnitude of G can be estimated from the photocurrent density at the transition to the saturation regime [1]. For a typical photovoltaic cell based on MDMO-PPV and PCBM, 2×10^{27} free electron-hole pairs are generated per second and cubic meter, upon illumination with 800 W/m^2 from a halogen lamp.

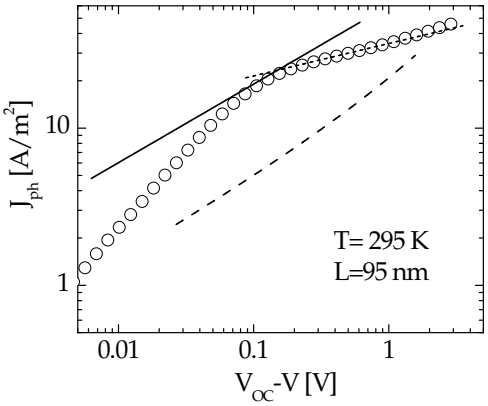

Figure 2.6: Photocurrent-voltage dependence of an ITO/PEDOT:PSS/MDMO-PPV:PCBM/LiF/Al photovoltaic cell (circles). The dotted line indicates the saturation current. The dashed line is the space-charge-limited photocurrent calculated using the μ_h of pristine MDMO-PPV and generation rate of free electron-hole pairs of 2×10^{27} m^{-3}s^{-1}. The continuous line is the space-charge-limited photocurrent calculated by assuming μ_h=10^{-8} m^2/Vs.

In Figure 2.6, the maximal electrostatically allowed photocurrent density, calculated by considering the reported hole mobility of pristine MDMO-PPV, is plotted (dashed line) as function of the effective voltage V_{OC}-V. The open-circuit voltage V_{OC} is the voltage at which the J_{ph} equals zero (after correction for the dark current), implying that the electric field in the device is small. The difference between the applied voltage V and V_{OC} therefore represents the effective voltage across the device. Surprisingly, the experimentally observed photocurrent (circles) of the photovoltaic cell exceeds its predicted limit by one order of magnitude. This raises the fundamental question: why the space-charge limit does not hold? Considering Equation 2.11, it appears that the experimentally observed photocurrent is only electrostatically allowed when the hole mobility in the blend exceeds 10^{-8} m^2/Vs (solid line), which is more than two orders of magnitude above the hole mobility of the pristine polymer. In this section, first the electron mobility in a 20:80 weight percentage (wt. %) blend of MDMO-PPV and PCBM is estimated from current-voltage measurements. Subsequently, the hole mobility in the blend is determined using current-voltage, transient electroluminescence (EL), and admittance spectroscopy measurements.

2.3.2 Electron transport in polymer:fullerene films

Prior the determination of the hole mobility, the electron mobility in a 20:80 wt. % MDMO-PPV:PCBM is investigated. In Figure 2.7, the experimental current density J_D of an ITO/PEDOT:PSS/MDMO-PPV:PCBM/LiF/Al diode with thickness L=170 nm is shown, together with the electron current density for a 170-nm-thick ITO/PEDOT:PSS/ PCBM/LiF/Al device. The applied bias V has

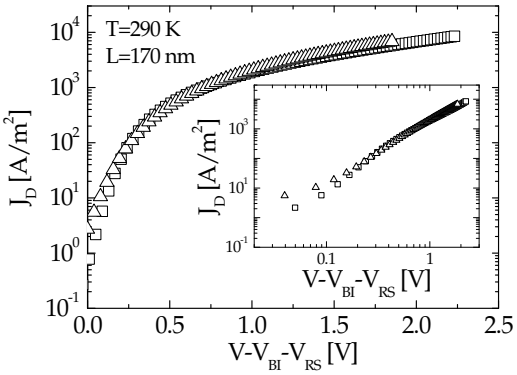

Figure 2.7: Experimental J_D-V characteristics of an ITO/PEDOT:PSS/MDMO-PPV:PCBM (20:80 wt. %)/LiF/Al diode in the dark (squares), together with a PCBM electron only device (triangles) with a thickness of L=170 nm, at a temperature T=290 K. The J_D-V characteristics are corrected for voltage drop across the ITO serial resistance V_{RS} (RS≈11 Ω) and for a built-in voltage (V_{BI}=1.4 V) that arises from the work function difference between the contacts. The inset shows the same data in a log-log plot to demonstrate that the current density depends quadratically on the voltage, characteristic for SCLC.

been corrected for the built-in voltage (V_{BI}=1.4 V) that arises from the work function difference between the ITO/PEDOT:PSS and LiF/Al contacts. For large current densities (larger than 1000 A/m^2), the applied voltage has also been corrected for the voltage drop across the ITO series resistance (V_{RS}), which is typically 11 Ω in these experiments. The slope of the log(J_D)-log(V) plot (inset of Figure 2.7) demonstrates that the current density depends quadratically on the voltage ($J_D \propto V^2$), consistent with SCLC. It appears from Figure 2.7 that in forward bias the dark current in MDMO-PPV:PCBM (20:80 wt. %) bulk heterojunction diodes is equal to the electron current in pristine PCBM. The fact that the experimental J_D-V curve of the bulk heterojunction diode lies on top of the PCBM device indicates that dark current of the blend is governed by electrons and the electron mobility of PCBM in the bulk heterojunction is not significantly affected by the presence of MDMO-PPV up to 20 wt. %. Furthermore, the SCLC behavior of PCBM demonstrates that the use of LiF/Al does not represent a significant barrier for electron injection. In order to investigate the hole current in a MDMO-PPV:PCBM bulk heterojunction diode, the electron current needs to be strongly suppressed. In the following, this type of devices are used to measure the transport of holes in the MDMO-PPV phase of the blend.

2.3.3 Hole transport in polymer:fullerene films

Current-voltage measurements

A frequently used tool for investigating charge-carrier mobilities of low mobility media is to examine the space-charge-limited current through the semiconduc-

tor in the dark [8], since the SCLC is directly proportional to the charge-carrier mobility (Equation 2.5).

As is demonstrated above, the electrons dominate the transport through the cell and the effective electron mobility in the cell equals the electron mobility in pristine PCBM (μ_e=2×10^{-7} m^2/Vs; as determined in Section 2.2). Consequently, in order to investigate the hole transport through the MDMO-PPV phase in the blend, the electron current through the PCBM phase has to be blocked, for example, by the choice of a high work function cathode (such as gold). However, it has been reported that still substantial injection-limited electron current flows when electrons are injected from gold into PCBM [23, 24], exceeding the typically observed hole current in devices of pristine MDMO-PPV. For that reason, it has been assumed that the hole mobility in a blend cannot be determined by examining current densities through devices with gold electron-blocking contacts [23]. From the analysis of injection-limited currents and open-circuit voltages of single-layer PCBM devices, it has been calculated that silver, gold, and palladium form barriers for electron injection of 0.65, 0.76, and 0.94 eV with PCBM, respectively [24]. Moreover, due to large electron injection barrier from palladium into PCBM, the experimental current that flows through an ITO/PEDOT:PSS/PCBM/Pd device is strongly suppressed, being comparable or below the leakage current of the device. As a result, palladium is the best alternative to block electron injection in the blend.

In Figure 2.8, the J_D-V characteristic of an ITO/PEDOT:PSS/MDMO-PPV:PCBM/Pd device is shown (circles). Note that the applied voltage is corrected for the built-in voltage V_{BI}. The built-in voltage results from the difference in the work function of the anode and the cathode [24]. Surprisingly, the J_D-V characteristics of the blend not only exceeded the calculated SCLC of single-

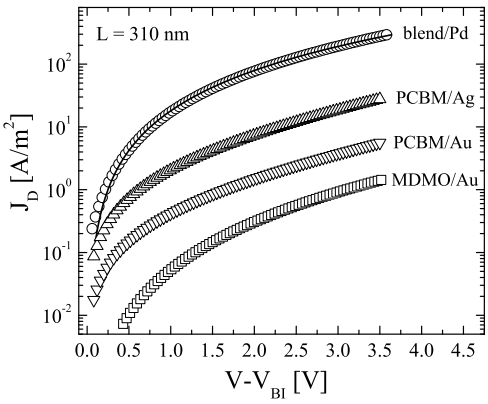

Figure 2.8: J_D-V characteristics of an ITO/PEDOT:PSS/MDMO-PPV:PCBM/Pd device(circles). The line is a fit using the model of single-carrier SCLC with a field-dependent mobility. Calculated electron-injection currents through ITO/PEDOT:PSS/PCBM/cathode devices with Ag (△) and Au (▽) as the cathode. Parameters were taken from reference [24]. Hole-only SCLC through MDMO-PPV (□) were calculated with the parameters previously determined by Blom et al. [8].

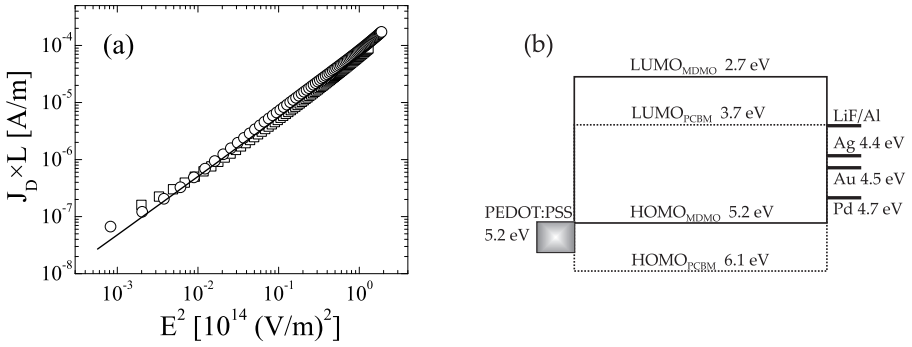

Figure 2.9: (a) J_D-V characteristics of an ITO/PEDOT:PSS/MDMO-PPV:PCBM/Pd (□) and an ITO/PEDOT:PSS/MDMO-PPV:PCBM/Ag (◯) device. The line is a fit using the model of single-carrier SCLC with a field-dependent mobility. (b) The energy band diagrams of a solar cell with various cathode metals [24].

layer MDMO-PPV hole-only device (□), but also exceeded the calculated electron injection-limited currents from silver (△) and gold (▽) into PCBM, which are both better electron injectors than palladium. There are two possible explanations for this strongly enhanced current in the blend. First, the observed current is a hole-only current, meaning that the hole mobility is strongly enhanced compared to that of pristine MDMO-PPV. Secondly, the observed current is an electron current and the injection-limited electron current from palladium into PCBM is strongly enhanced by the presence of holes, and was therefore not comparable to the injection-limited electron current observed with single-layer PCBM devices.

Whether or not the observed current densities in the blend were influenced by electron injection from the cathode into PCBM was verified by changing the cathode metal, thereby altering the charge-injection barriers. In Figure 2.9(a), it is shown that the current through a device based on a blend remains unchanged, even when the cathode is changed from palladium to silver. A schematic band diagram is shown in the Figure 2.9(b). Consequently, any contribution of electrons to the current is highly unlikely, and, in the analysis of the J_D-V characteristics, we regard the device as a hole-only device.

The current densities obtained from an ITO/PEDOT:PSS/MDMO-PPV:PCBM /Pd device scale quadratically with the applied voltage [Figure 2.9(a)], which is indicative of space-charge limited transport. Assuming that the device is hole-dominated, the J_D-V measurements thus provide information on the hole mobility of the MDMO-PPV phase in the blend. Similar to the findings in pristine MDMO-PPV [8] and PCBM (Section 2.2), the hole mobility was field-dependent in a stretched exponential form, as given by the Equation 2.4. By simulating the SCLC of the hole-only devices of Figure 2.9(a), a zero-field mobility for holes in MDMO-PPV phase of the blend of $\mu_h = 1.5 \times 10^{-8}$ m^2/Vs and a field activation factor $\gamma_h = 1.4 \times 10^{-4}$ m$^{1/2}$/V$^{1/2}$ were obtained at room temperature.

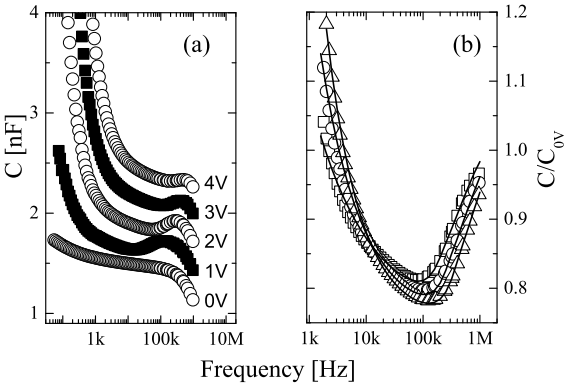

Figure 2.10: (a) Capacitance-frequency plot of an ITO/PEDOT:PSS/MDMO-PPV:PCBM /Pd device at different DC bias. The respective capacitance traces are offset for clarity. The layer thickness was 310 nm. (b) Capacitance normalized to zero DC bias capacitance versus frequency for 3 V (□), 3.5 V (◯), and 4 V (△) DC bias. The lines are fits with the admittance model for space-charge limited conduction given by Martens et al. [10].

Admittance spectroscopy

A powerful technique for investigating charge transport in conjugated polymers is admittance spectroscopy. This technique has already been used for determining transit times (τ_t) and, hence, charge carrier mobilities of pristine MDMO-PPV [10]. In a diode, where direct currents (DC) are space-charge limited, a small alternating current (AC) disturbance of the DC bias changes the space-charge density in the semiconductor, if the frequency ω is below τ_t^{-1}. The space-charge build-up is delayed with respect to the AC stimulus, resulting in an inductive contribution to the capacitance. For frequencies $\omega > \tau_t^{-1}$, the additional space-charge build-up can not fallow the AC stimulus and the geometric capacitance is measured. Consequently, τ_t of the charge carriers is given by the threshold frequency, below which a reduction in capacitance is observed. An advantage of this technique is that for devices where both electrons and holes are present, such as in the case of MDMO-PPV-based light-emitting diodes, the respective transport properties can be individually monitored, since they are separated in frequency space [25].

In Figure 2.10, it is shown by admittance measurements that ITO/PEDOT:PSS /MDMO-PPV:PCBM/Pd devices exhibit a capacitance decrease below a certain threshold frequency. The fact that an inductive contribution to the capacitance was present confirms that the DC currents through these devices were space-charge limited. For a strongly injection-limited device the amount of injected charge is too small to exhibit an inductive contribution to the capacitance. The observed threshold frequency shows a clear trend upon changes in DC bias. By increasing the DC bias, the threshold frequency was shifted to higher frequencies, reflecting a reduction of the transit time of the charge carriers. From the frequency response of the capacitance, the transit times were determined

by simulating the capacitance frequency dependence with a model for space-charge limited admittance [10]. The resulting hole mobilities in the MDMO-PPV phase of the blend for different DC fields are depicted in Figure 2.12. They are in excellent agreement with the mobilities obtained by simulating the DC SCLC (Figure 2.9). Since the mobility of the electrons in the blend can be estimated [23], the threshold frequency for electron transport can be predicted, and is typically one order of magnitude above the observed threshold frequencies. The absence of any inductive contribution at these higher frequencies is indicative of a hole-dominated device.

Transient Electroluminescence

As a final proof that the transport in the investigated devices was dominanted by holes, and that it is conceivable that the SCLC and admittance spectroscopy unveiled the hole mobility in the MDMO-PPV phase, a modified transient electroluminescence (EL) technique was applied. Transient EL has frequently been used to estimate charge-carrier mobilities in highly luminescent organic thin films [9, 26–28]. Upon applying a rectangular voltage pulse to a diode, holes and electrons are injected at the corresponding electrodes and traverse the luminescent organic semiconductor until they meet and radiative recombination occurs. A time delay between the onset of the applied voltage and the appearance of the EL is directly related to the transit times of the charge carriers. Advantage can be taken of the fact that hole mobilities in PPV-type materials typically exceed the electron mobilities [27, 29, 30]. The delay between voltage onset and the appearance of the EL is, therefore, primarily related to the τ_t of the faster charge-carrier species.

As desired in photovoltaic cells, the luminescence in a blend of MDMO-PPV and PCBM is strongly quenched, which complicates the determination of the transit times with EL transient measurements. However, by introducing a luminescent layer between the blend and the cathode, this difficulty can be circumvented. In such double-layer diodes, holes are injected from the anode into the MDMO-PPV phase of the blend and electrons are injected from the cathode into the luminescent layer, as shown schematically in the inset of Figure 2.11. Since radiative recombination exclusively occurs in the luminescent layer, holes have to traverse the entire blend in order to participate in the recombination. Assuming a low electron mobility in the luminescent layer, the time delay between the EL signal and the stimulus (τ_t^{total}) is given by the transit times of holes passing the blend (τ_t^{blend}) and the luminescent layer (τ_t^{lum}):

$$\tau_t^{total} = \tau_t^{blend} + \tau_t^{lum} \tag{2.12}$$

The PPV-based oligomer (E,E,E,E)-1,4-bis[(4-styryl)styryl]-2-methoxy-5-(2' -ethylhexyloxy)benzene (MEH-OPV5) was used as the luminescent layer, since its highest occupied molecular orbital (HOMO) matches that of MDMO-PPV and its electron mobility is known to be below its hole mobility [28, 31]. Furthermore, because MEH-OPV5 can be deposited by thermal vacuum deposition, intermixing of the blend and the MEH-OPV5 cover layer is prevented. A high

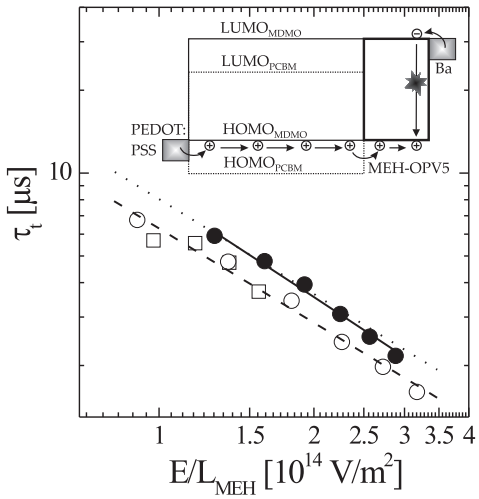

Figure 2.11: Transit times of holes from EL transient measurements for ITO/PEDOT:PSS/ MEH-OPV5/Ba devices with 100 nm (◯) and 160 nm (□) layer thickness and an ITO/PEDOT:PSS /MDMO-PPV:PCBM/MEH-OPV5/Ba device with 200 nm layer thickness of the blend and 60 nm layer thickness (L_{MEH}) of MEH-OPV5 (•). The dashed line is a fit using $\tau_t \propto (L/E)^{1/\alpha}$. The dotted line indicates the transit times of double-layer diodes with transport dispersion in the MEH-OPV5 layer, but no dispersion in the blend and a constant hole mobility. The continuous line is a fit using Equations 2.12 and 2.13 with field-dependent mobility given by the Equation 2.4. The inset schematically shows the operation principle of the EL transient technique in the double-layer configuration.

EL brightness at low bias was guaranteed by using PEDOT:PSS as the anode and barium as the cathode.

In order to investigate the transit times of charge carriers passing the blend in a double-layer arrangement, the transit times through the MEH-OPV5 film were first investigated. In Figure 2.11, the transit times for single-layer MEH-OPV5 devices are shown for film thicknesses of 100 and 160 nm (empty symbols). The revealed transit times are in agreement with those previously reported [28]. The field and thickness dependence of the transit times could be described by $\tau_t \propto (L/E)^{1/\alpha}$ with $\alpha \approx 0.88$, indicating weak dispersivity of the hole transport in MEH-OPV5 [32].

The EL spectrum obtained from a double-layer diode of the blend and MEH-OPV5 was equal to the emission spectrum of a pure MEH-OPV5 layer, confirming that holes did indeed travel through the entire blend. For a double-layer diode with a total thickness of 260 nm, the measured transit times (Figure 2.11, solid symbols) were, however, only slightly longer than those found for the single-component MEH-OPV5 film. This suggests that the transit times of charge carriers passing the blend were even shorter than those of charge carriers

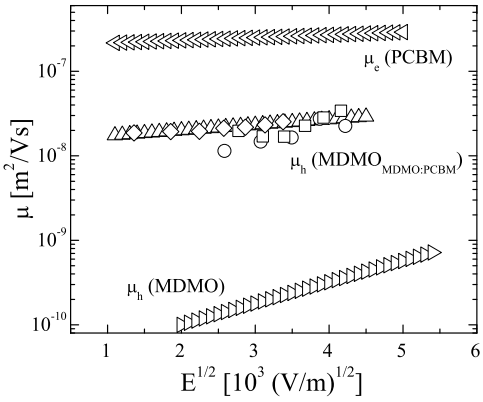

Figure 2.12: Charge carrier mobilities versus the square-root of the electric field. The hole mobility of pristine MDMO-PPV was taken from Blom et al. [8] and the electron mobility of pristine PCBM was determined in Section 2.2 of this thesis. The hole mobilities of the MDMO-PPV phase in the blend with PCBM were obtained by examining the SCLC of hole-only devices (△), by admittance spectroscopy (⋄), and by EL transient measurements for 200 nm (□) and 120 nm (◯) layer thickness of the blend and 60 nm MEH-OPV5.

passing the MEH-OPV5 layer. If we convert the observed transit times for the blend directly into a mobility using Equation 2.13,

$$\mu_h = \frac{L_{blend}}{\tau_t^{blend} E}, \tag{2.13}$$

it appears from Figure 2.12 (□ and ◯) that the obtained hole mobilities are close to those found with both DC J_D-V measurements and admittance spectroscopy. This indicates that the hole transport through the blend is not (or only slightly) dispersive. The accordance between mobilities obtained from transient EL measurements and mobility unveiled by J_D-V and admittance measurements is conclusive proof that the charge transport in ITO/PEDOT:PSS/MDMO-PPV:PCBM/Pd devices is hole-dominated and enhanced.

Discussion

A remarkable agreement between the hole mobilities obtained from DC J_D-V measurements, admittance spectroscopy, and transient EL measurements has been observed (Figure 2.12). Accordingly, the room temperature hole mobility in the blend of MDMO-PPV and PCBM is 2×10^{-8} m^2/Vs for an electric field of 4×10^6 V/m, which is only one order of magnitude lower than the respective electron mobility in pristine PCBM and 200-fold higher than the hole mobility in the pristine polymer. A changed hole mobility in donor-like polymers upon blending with PCBM has already been reported [33, 34]. The charge carrier mobilities in the blend of MDMO-PPV and PCBM were measured, for instance,

by Choulis et al., using time-of-flight photocurrent measurements [34]. They reported that the hole mobility in the MDMO-PPV phase of a blend decreases upon adding PCBM below its percolation threshold from 2.4×10^{-10} m^2/Vs to 2.3×10^{-11} m^2/Vs at 2.2×10^7 V/m and increase again above the percolation threshold of PCBM to approximately 2×10^{-10} m^2/Vs for a blend of 20:80 wt. % of MDMO-PPV:PCBM. Nonetheless, the hole mobility was found to be far below the measured electron mobility in PCBM (see Section 2.2). Hence, it was believed that space-charge effects restrain the photoresponse of a photovoltaic cell, which is, however, in contradiction to the observed photocurrents (Figure 2.6). Since, for example, a photocurrent governed by square-root dependence on V (Equation 2.11) does not allow fill factors larger than ≈40%, the typically observed fill factors of 60% [4] are inaccessible in the space-charge limit. Yet, the hole mobility reported herein is consistent with the reported photoresponse of a cell, exceeding the minimum hole mobility of 10^{-8} m^2/Vs, which is required for the electrostatically allowed photocurrent. Space-charge effects and the concomitant charge carrier recombination, hence, do not limit the photoresponse, and fill factors of 60% are conceivable. The discrepancy between the hole mobilities reported here and those of Choulis et al. might be related to differences in the film morphology arising from differences in the sample preparation, which are essential for obtaining the desire device. Whereas a layer of 1 μm was required for transient photocurrent measurements, the devices we investigated exhibited a layer thickness equal to or smaller than 300 nm, coming closer to the device thickness that is usually used in the photovoltaic cells.

Why the hole mobility in the MDMO-PPV increases upon blending the polymer with an excess of PCBM remains an unsolved question. Recently, it has been demonstrated that the charge carrier mobility in MDMO-PPV as extracted from hole-only diodes and field-effect transistors can differ by more than three orders of magnitude [12]. This large difference originates from the strong dependence of the mobility on charge carrier density. However, in the space-charge limited device investigated herein, the carrier densities are low and this effect can not be responsible for the observed mobility increase upon blending with PCBM. Pacios et al. proposed that a change in film morphology upon increased PCBM concentration results in an enhanced intermolecular interaction and, hence, in

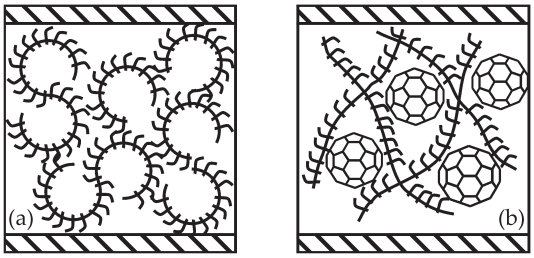

Figure 2.13: (a) The molecular conformation of pristine MDMO-PPV according to Kemerink et al. [35]. (b) Upon mixing MDMO-PPV with PCBM interactions between the two moieties might change the molecular conformation of MDMO-PPV.

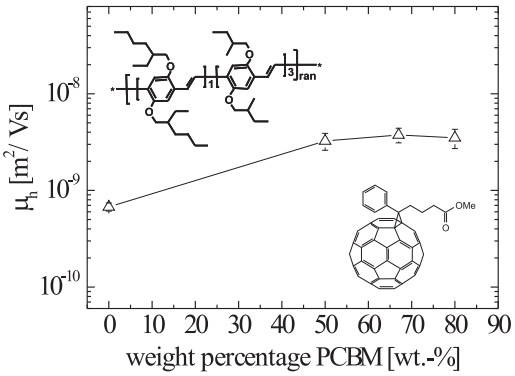

Figure 2.14: Hole mobility (μ_h) of a symmetrical substituted PPV (BEH_1BMB_3-PPV) as a function of weight percentage PCBM in the PPV:PCBM blend films. The inset shows the chemical structures of symmetrical substituted PPV (upper image) and PCBM (lower image).

an improved charge transfer between adjacent molecules [33]. Recent observation on the molecular level concerning the film morphology of MDMO-PPV suggest a similar scenario. It was found that films of MDMO-PPV exhibit interconnected ring-like features, which were attributed to ring-like bent chains, as schematically depicted in Figure 2.13(a) [35].

The molecular conformation was understood in terms of interactions between adjacent aliphatic side chains on one single chain. Due to the asymmetric side-chain substituents in MDMO-PPV, the interaction causes a bending of the otherwise rigid polymer backbone. Hence, a conformation of the polymer, where the substituents of the same species preferably point to one side of the backbone, results in a circular bending of the chain. It has been shown that ring-like, bent polymer chains randomly stack in a pronounced two-dimensional manner. The relevant molecular conformation and the weakly ordered stacking of the molecules might be the origin of the poor transport properties of the pristine MDMO-PPV, since they are likely to result in a high disorder energy and in poor π-π interaction. However, upon blending MDMO-PPV with PCBM, the situation might change, that is, when the formation of the ring-like molecular conformation is hindered due to interactions between MDMO-PPV and PCBM [Figure 2.13(b)]. On the basis of this assumption, an improvement in the charge transport properties can be expected, resulting from a reduced nearest-neighbor hopping distance and/or a lower disorder energy. From temperature-dependent measurements, a change in the disorder energy of 0.01 eV could be estimated. Whether this explanation can predict an increase in the hole mobility of more than two orders of magnitude, however, is not clear at present. Modifying the hole-transport properties by systematically changing the chemical structure of the donor-like polymers as well as the PCBM concentration in the blend might give an answer to this question.

The morphology studies also revealed that the chains of a symmetrically substituted polymer show a linear orientation in the film [35]. Therefore, we

have further investigated the hole mobility in a symmetrical substituted PPV and PCBM blends. The PPV used in this investigation is a random co-polymer poly[2,5-bis(2'-ethylhexyloxy)-co-2,5-bis(2'-methylbutyloxy)-1,4-phenylene vinylene] (BEH_1BMB_3-PPV), with its chemical structure shown in the inset of Figure 2.14. For this symmetrically substituted PPV, when blended with PCBM at different weight percentages, we observe that the hole mobility in the PPV phase is hardly affected compared with that measured in pristine PPV, as shown in Figure 2.14. This indicates that the molecular conformation of the MDMO-PPV in the presence of PCBM is the reason for the enhanced hole mobility measured in these blends.

2.3.4 Conclusion

In this section, the electron and hole mobility in 20:80 weight percentage blends of MDMO-PPV:PCBM is determined. It is shown that the electrons dominate the transport through the cell and that the effective charge-carrier mobility in the cell equals the electron mobility in pristine PCBM (μ_e=2$\times 10^{-7}$ m^2/Vs). With respect to hole mobility, we have presented consistent experimental evidence that, upon blending MDMO-PPV with PCBM, the hole mobility in the MDMO-PPV phase is enhanced by more than two orders of magnitude, compared to the pristine polymer. A hole mobility of around 2×10^{-8} m^2/Vs was disclosed, which is only one order of magnitude lower than the electron mobility in PCBM. Consequently, the charge transport in a bulk heterojunction solar cell based on MDMO-PPV and PCBM is much more balanced than earlier believed and space-charge build-up is therefore not limiting the photoresponse. These results shine new light on the high external quantum efficiencies observed in these photovoltaic cells.

2.4 Experimental section

Device Preparation: Prepatterned ITO-coated glass substrates were wet-cleaned by rubbing with soap, rinsing with water, and ultrasonic cleaning in acetone and 2-propanol. The substrates were further UV-ozone treated and a layer of PEDOT:PSS (Bayer AG) was subsequently spin-coated on the pre-cleaned ITO, using a Convac spin-coater. The PEDOT:PSS layer was dried at an elevated temperature. The samples were then inserted into a glove box filled with nitrogen. A thin layer of a blend of MDMO-PPV:PCBM in a 20:80 wt. % was then spin-coated from a chlorobenzene solution (with a concentration of $\approx$3.3 to 6 mg PPV/mL) using a Karl Suss spin-coater. The pristine PCBM samples used to investigate electron mobility in Section 2.2 were spin-coated in air, at room temperature, from a chlorobenzene solution with a concentration of about 30 mg/mL. For transient EL measurements, a thin MEH-OPV5 layer was subsequently vacuum-deposited at 10^{-6} mbar on the blend. Finally, top contacts were deposited via vacuum deposition at 10^{-7} mbar.
Device Characterization: All measurements were performed under a nitrogen atmosphere. J-V measurements were performed with a Keithley 2400

Sourcemeter and admittance spectroscopy with an Agilent 4284 A Precision LCR Meter. For transient EL measurements, an HP 8114 A Pulse Generator was used to apply step-like voltage pulses on the samples; the integrated light output was measured with a Keithley 6514 System Electrometer. A detailed description of the transient EL measurements has been given by Blom and Vissenberg [26].

References

[1] A. M. Goodman, A. Rose, *Double extraction of uniformly generated electron-hole pairs from insulators with noninjecting contacts*, Journal of Applied Physics **42** (1971), 2823.

[2] K. C. Kao, W. Hwang, *Electrical transport in solids with particular reference to organic semiconductors*, Pergamon Press **vol.14** (1970).

[3] C. J. Brabec, N. S. Sariciftci, J. C. Hummelen, *Plastic solar cells*, Advanced Functional Materials **11** (2001), 15.

[4] S. E. Shaheen, C. J. Brabec, N. S. Sariciftci, F. Padinger, T. Fromherz, J. C. Hummelen, *2.5% efficient organic plastic solar cells*, Applied Physics Letters **78** (2001), 841.

[5] J. M. Kroon, M. M. Wienk, W. J. H. Verhees, J. C. Hummelen, *Accurate efficiency determination and stability studies of conjugated polymer/fullerene solar cells*, Thin Solid Films **403** (2002), 223.

[6] N. S. Sariciftci, L. Smilowitz, A. J. Heeger, F. Wudl, *Photoinduced electron-transfer from a conducting polymer to buckminsterfullerene*, Science **258** (1992), 1474.

[7] C. J. Brabec, G. Zerza, G. Cerullo, S. De Silvestri, S. Luzzati, J. C. Hummelen, S. Sariciftci, *Tracing photoinduced electron transfer process in conjugated polymer/fullerene bulk heterojunctions in real time*, Chemical Physics Letters **340** (2001), 232.

[8] P. W. M. Blom, M. J. M. deJong, M. G. vanMunster, *Electric-field and temperature dependence of the hole mobility in poly(p-phenylene vinylene)*, Physical Review B **55** (1997), R656.

[9] M. C. J. M. Vissenberg, P. W. M. Blom, *Transient hole transport in poly(-p-phenylene vinylene) LEDs*, Synthetic Metals **102** (1999), 1053.

[10] H. C. F. Martens, H. B. Brom, P. W. M. Blom, *Frequency-dependent electrical response of holes in poly(p-phenylene vinylene)*, Physical Review B **60** (1999), R8489.

[11] M. C. J. M. Vissenberg, M. Matters, *Theory of the field-effect mobility in amorphous organic transistors*, Physical Review B **57** (1998), 12964.

[12] C. Tanase, E. J. Meijer, P. W. M. Blom, D. M. de Leeuw, *Unification of the hole transport in polymeric field-effect transistors and light-emitting diodes*, Physical Review Letters **91** (2003), 216601.

[13] C. Tanase, P. W. M. Blom, D. M. de Leeuw, E. J. Meijer, *Charge carrier density dependence of the hole mobility in poly(p-phenylene vinylene)*, Physica Status Solidi A-Applied Research **201** (2004), 1236.

[14] G. G. Malliaras, J. R. Salem, P. J. Brock, J. C. Scott, *Photovoltaic measurement of the built-in potential in organic light emitting diodes and photodiodes*, Journal of Applied Physics **84** (1998), 1583.

[15] M. A. Lampert, P. Mark, *Current injection in solids*, Academic Press, New York (1970).

[16] R. C. Haddon, A. S. Perel, R. C. Morris, T. T. M. Palstra, A. F. Hebard, R. M. Fleming, *C-60 thin-film transistors*, Applied Physics Letters **67** (1995), 121.

[17] E. Frankevich, Y. Maruyama, H. Ogata, *Mobility of charge carriers in vapor-phase grown C60 single crystal*, Chemical Physics Letters **214** (1993), 39.

[18] P. M. Borsenberger, D. S. Weiss, *Organic photoreceptors for imaging systems*, Dekker, New York (1993).

[19] H. Bässler, *Charge transport in disordered organic photoconductors - A monte-carlo simu-*

lation study, Physica Status Solidi B-Basic Research **175** (1993), 15.

[20] S. V. Novikov, D. H. Dunlap, V. M. Kenkre, P. E. Parris, A. V. Vannikov, *Essential role of correlations in governing charge transport in disordered organic materials*, Physical Review Letters **81** (1998), 4472.

[21] H. C. F. Martens, P. W. M. Blom, H. F. M. Schoo, *Comparative study of hole transport in poly(p-phenylene vinylene) derivatives*, Physical Review B **61** (2000), 7489.

[22] R. Sokel, R. C. Hughes, *Numerical-analysis of transient photoconductivity in insulators*, Journal of Applied Physics **53** (1982), 7414.

[23] J. K. J. van Duren, V. D. Mihailetchi, P. W. M. Blom, T. van Woudenbergh, J. C. Hummelen, M. T. Rispens, R. A. J. Janssen, M. M. Wienk, *Injection-limited electron current in a methanofullerene*, Journal of Applied Physics **94** (2003), 4477.

[24] V. D. Mihailetchi, P. W. M. Blom, J. C. Hummelen, M. T. Rispens, *Cathode dependence of the open-circuit voltage of polymer:fullerene bulk heterojunction solar cells*, Journal of Applied Physics **94** (2003), 6849.

[25] H. C. F. Martens, J. N. Huiberts, P. W. M. Blom, *Simultaneous measurement of electron and hole mobilities in polymer light-emitting diodes*, Applied Physics Letters **77** (2000), 1852.

[26] P. W. M. Blom, M. C. J. M. Vissenberg, *Dispersive hole transport in poly(p-phenylene vinylene)*, Physical Review Letters **80** (1998), 3819.

[27] D. J. Pinner, R. H. Friend, N. Tessler, *Transient electroluminescence of polymer light emitting diodes using electrical pulses*, Journal of Applied Physics **86** (1999), 5116.

[28] C. Melzer, V. V. Krasnikov, G. Hadziioannou, *Charge transport, injection, and photovoltaic phenomena in oligo(phenylenevinylene) based diodes*, Journal of Polymer Science Part B: Polymer Physics **41** (2003), 2665.

[29] L. Bozano, S. A. Carter, J. C. Scott, G. G. Malliaras, P. J. Brock, *Temperature- and field-dependent electron and hole mobilities in polymer light-emitting diodes*, Applied Physics Letters **74** (1999), 1132.

[30] J. C. Scott, P. J. Brock, J. R. Salem, G. G. Malliaras, S. A. Carter, L. Bozano, *Charge transport processes in organic light-emitting devices*, Synthetic Metals **111** (2000), 289.

[31] S. C. Veenstra, U. Stalmach, V. V. Krasnikov, G. Hadziioannou, H. T. Jonkman, A. Heeres, G. A. Sawatzky, *Energy level alignment at the conjugated phenylenevinylene oligomer/metal interface*, Applied Physics Letters **76** (2000), 2253.

[32] H. Scher, E. W. Montroll, *Anomalous transit-time dispersion in amorphous solids*, Physical Review B **12** (1975), 2455.

[33] R. Pacios, D. D. C. Bradley, J. Nelson, C. J. Brabec, *Efficient polyfluorene based solar cells*, Synthetic Metals **137** (2003), 1469.

[34] S. A. Choulis, J. Nelson, Y. Kim, D. Poplavskyy, T. Kreouzis, J. R. Durrant, D. D. C. Bradley, *Investigation of transport properties in polymer/fullerene blends using time-of-flight photocurrent measurements*, Applied Physics Letters **83** (2003), 3812.

[35] M. Kemerink, J. K. J. van Duren, P. Jonkheijm, W. F. Pasveer, P. M. Koenraad, R. A. J. Janssen, H. W. M. Salemink, J. H. Wolter, *Relating substitution to single-chain conformation and aggregation in poly(p-phenylene vinylene) films*, Nano Letters **3** (2003), 1191.